

Measurement of the Very Forward Photon Spectrum in Deep-Inelastic Scattering at HERA

H1 Collaboration

Abstract

The production of photons at very low angles is studied in deep-inelastic positron-proton scattering at HERA. The data are taken with the H1 detector in the years 2006 and 2007 and correspond to an integrated luminosity of 126 pb^{-1} . Cross sections are measured for photon virtualities $6 < Q^2 < 100 \text{ GeV}^2$ and inelasticity $0.05 < y < 0.6$ as a function of longitudinal momentum fraction x_L^{lead} and transverse momentum p_T^{lead} of the most energetic photon. In addition, the cross sections are studied as a function of the sum of the longitudinal momentum fraction x_L^{sum} of all photons in the pseudorapidity range $\eta > 7.9$. The cross sections are normalised to the inclusive deep-inelastic scattering cross section. The measurements are compared to Monte Carlo predictions of deep-inelastic scattering models and the hadronic interaction models of high-energy cosmic rays.

1 Introduction

Measurements of very forward particle production in electron-proton collisions provide an important input for improving the theoretical understanding of the proton fragmentation mechanisms. The H1 and ZEUS experiments at the ep collider HERA have published several analyses on the production of forward¹ protons and neutrons which carry a large fraction of the longitudinal momentum of the incoming proton [1–9]. The analyses demonstrate that the Monte Carlo models are able to reproduce these measurements if they include contributions from string fragmentation, pion exchange and diffractive dissociation of the proton. These measurements are also valuable for the physics of ultra-high energy cosmic rays, as they can help to reduce the uncertainties in the model predictions for very high energy cosmic ray showers.

This paper presents studies made by the H1 experiment of Deep-Inelastic Scattering (DIS) interactions in which one or more photons are produced at very small polar angles θ below 0.75 mrad and measured in the forward neutron calorimeter (FNC). The dominant source of forward photons is the decay of π^0 -mesons. At high energies, both photons from the π^0 decay can be detected by the FNC. However, due to the limited geometrical acceptance, these photons, as well as photons produced from other sources, cannot be distinguished in the FNC and are reconstructed as a single particle (see section 3.1 for details).

This is a first measurement of very forward photons at HERA. It was made possible due to the upgrade of the H1 FNC calorimeter which included a new electromagnetic section.

2 Cross Section Definition and Models

Cross sections are presented differentially in several kinematic variables sensitive to the underlying physics process. The variables x_L^{lead} and p_T^{lead} are the longitudinal momentum fraction and transverse momentum of the most energetic photon in the energy range $0.1 < x_L < 0.7$ and pseudorapidity range $\eta > 7.9^2$. Here, the longitudinal momentum fraction $x_L \simeq E_\gamma/E_p$ of a given photon is calculated with respect to the proton beam energy E_p . In addition, measurements are made differentially in $x_L^{sum} = \sum x_L$, corresponding to the sum of photons in the same pseudorapidity range $\eta > 7.9$.

The measurements are compared with the predictions of hadronic fragmentation models used in DIS simulations implemented in the DJANGO [10] program (see section 3.3 for details). The measurements are compared also with the predictions of hadronic interaction models which are commonly used for the simulation of cosmic ray cascades, EPOS [11], QGSJET 01 [12, 13], QGSJET II [14, 15] and SIBYLL [16, 17]. These phenomenological models based on general principles such as unitarity and analyticity of scattering amplitudes are combined with perturbative QCD predictions for high- p_T processes to obtain a description of the final states.

¹The origin of the right-handed H1 coordinate system is the nominal ep interaction point. The direction of the proton beam defines the positive z -axis (forward direction); the polar angle θ is measured with respect to this axis. Transverse momenta are measured in the x - y plane.

²The pseudorapidity is defined by $\eta = -\ln(\tan \frac{\theta}{2})$. Pseudorapidity range $\eta > 7.9$ corresponds to the range of polar angle $\theta < 0.75$ mrad.

3 Experimental Procedure and Data Analysis

The data used in this analysis were collected with the H1 detector at HERA in the years 2006 and 2007 and correspond to an integrated luminosity of 126 pb^{-1} . For the period used in the analysis, HERA collided positrons and protons with energies of $E_e = 27.6 \text{ GeV}$ and $E_p = 920 \text{ GeV}$, respectively, corresponding to an ep centre of mass energy of $\sqrt{s} = 319 \text{ GeV}$.

3.1 Detection of forward neutral particles

Neutral particles scattered at very low angles can be detected in the FNC calorimeter, which is installed 106 m from the interaction point at a polar angle of 0° in the proton beam direction. A schematic view of the H1 FNC used during the HERA-II running period (2002-2007) is shown in Fig. 1a. A detailed description of the FNC is given in [9]. It consists of the Main Calorimeter and the Preshower Calorimeter situated directly in front of the Main Calorimeter. In addition, two layers of veto counters situated at a distance of 2 m in front of the Preshower Calorimeter are used to veto charged hadrons.

The Main Calorimeter of the FNC is a sandwich-type calorimeter consisting of four identical sections of 51.5 cm long sensitive volume and transverse dimensions of $60 \times 60 \text{ cm}^2$. The total length of the Main Calorimeter is 8.9 nuclear interaction lengths. The Preshower Calorimeter is a 40 cm long lead–scintillator sandwich calorimeter. The length corresponds to about 60 radiation lengths. The Preshower Calorimeter is composed of 24 planes: the first 12 planes each consist of a lead plate of 7.5 mm thickness and a scintillator plate of 2.6 mm thickness. The second 12 planes each consist of a lead plate of 14 mm thickness and a scintillator plate of 5.2 mm thickness. The transverse size of the scintillating plates is $26 \times 26 \text{ cm}^2$. Each scintillating plate has 45 grooves with 1.2 mm wavelength shifter fibres attached down one side. The orientation of fibres alternates from horizontal to vertical in consecutive planes. At each plane, the fibres are bundled into nine strips of five fibres. Longitudinally, the strips are combined into 9 vertical and 9 horizontal towers which are finally connected to 18 photomultipliers.

The acceptance of the FNC is defined by the aperture of the HERA beam-line magnets and is limited to scattering angles of $\theta \lesssim 0.8 \text{ mrad}$ with approximately 30% azimuthal coverage. The geometrical acceptance window of the FNC is shown in Fig. 1b together with the layout of the Preshower readout strips.

The small geometrical acceptance window combined with the relatively large size of the FNC readout modules means that showers from two or more particles which enter the FNC are reconstructed as a single cluster.

The longitudinal segmentation of the FNC allows efficient discrimination of photons from hadrons. The photon reconstruction algorithm is based on the fact that the electromagnetic showers are fully contained in the Preshower Calorimeter while the energy deposit in the Main Calorimeter is compatible with the noise level. For high energy neutrons the largest fraction of energy is contained in the Main Calorimeter. However, low energy neutrons deposit large fractions of their energy in the Preshower. The fraction of neutrons which can be misidentified as photons is about 35% for neutrons with energies below 100 GeV, decreasing to 2% for neutrons with energy in the range between 100 and 200 GeV.

The detection and reconstruction efficiency for forward photons estimated from Monte Carlo simulation is about 85% at low energies increasing to 95% at high energies. Losses are mainly due to interactions with the beampipe.

The energy resolution of the FNC calorimeter for electromagnetic showers is $\sigma(E)/E \approx 20\%/\sqrt{E}$ [GeV]. The spatial resolution for electromagnetic showers and for those hadronic showers which started to develop in the Preshower Calorimeter is about 2 mm.

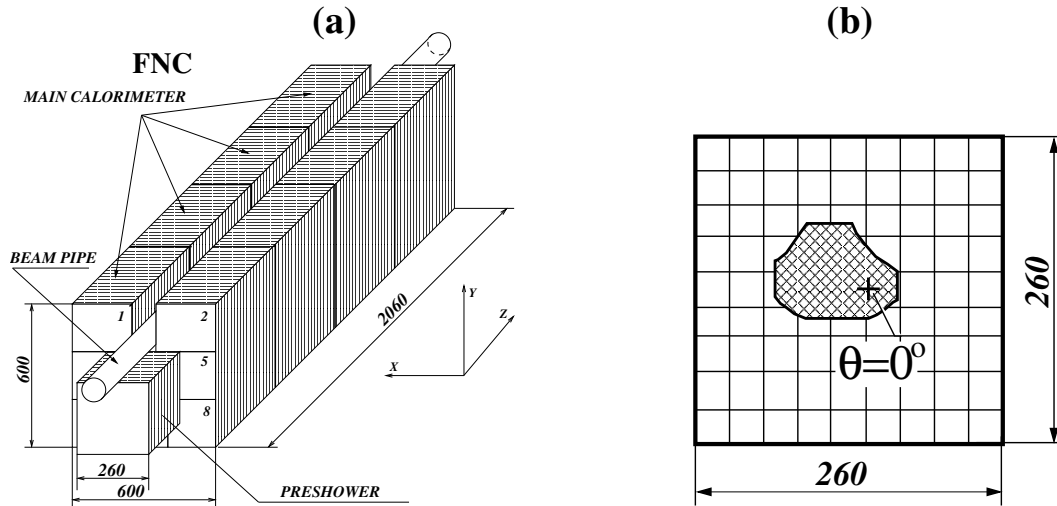


Figure 1: (a) A schematic view of the H1 FNC. (b) Layout of readout strips of the Preshower Calorimeter. The hatched area shows the geometrical acceptance window defined by the beam-line elements. The position corresponding to $\theta = 0^\circ$ is also indicated. All dimensions are given in mm.

3.2 Event selection

The data sample of this analysis was collected using triggers which require the scattered positron to be measured in the SpaCal. The trigger efficiency is close to 96% for the analysis phase space as determined from data using independent triggers.

The selection of DIS events is based on the identification of the scattered positron as the most energetic compact calorimetric deposit in the SpaCal with an energy $E'_e > 11$ GeV and a polar angle $156^\circ < \theta'_e < 175^\circ$. The energy weighted cluster radius is required to be less than 4 cm, as expected for an electromagnetic shower. The z -coordinate of the primary event vertex is required to be within ± 35 cm of the nominal position of the interaction point. To suppress events with initial state hard photon radiation, as well as events originating from non- ep interactions, the quantity $E - p_z$, summed over all reconstructed particles including the positron, is required to lie between 35 GeV and 70 GeV. This quantity, which refers to the energy and longitudinal momentum component of each final state particle, is expected to be twice the electron beam energy for fully contained events. In addition, events are restricted to the kinematic range $6 < Q^2 < 100$ GeV² and $0.05 < y < 0.6$. Here the four-momentum transfer squared Q^2 and the inelasticity y are the Lorentz invariant kinematic variables used to describe high energy ep interactions. These are determined from the energies E_e and E_p of

the lepton and proton beams, respectively, and from the energy E'_e and polar angle θ'_e of the scattered lepton in the laboratory frame as

$$Q^2 = 4E_e E'_e \cos^2 \left(\frac{\theta'_e}{2} \right); \quad y = 1 - \frac{E'_e}{E_e} \sin^2 \left(\frac{\theta'_e}{2} \right). \quad (1)$$

Events containing forward photons are selected by requiring an electromagnetic cluster in the FNC with an energy above 92 GeV and a polar angle below 0.75 mrad. About 0.8% of selected DIS events satisfy the forward photon selection criteria.

3.3 Monte Carlo simulations and corrections to the data

Monte Carlo (MC) simulations are used to correct the data for the effects of detector acceptance, inefficiencies, migrations between measurement intervals due to finite detector resolution and QED radiation from the positron. All generated events are passed through a GEANT3 [18] based simulation of the H1 apparatus and are then passed through the same reconstruction and analysis chain as is used for the data.

The DJANGO [10] program generates inclusive DIS events. It is based on leading order electroweak cross sections and takes QCD effects into account up to order α_s . Higher order QCD effects are simulated using LEPTO 6.5 [19], based on leading log parton showers, or using the Colour Dipole Model (CDM) as implemented in ARIADNE [20]. Subsequent hadronisation effects are modelled using the Lund string fragmentation model as implemented in JETSET [21]. Higher order electroweak processes are simulated using an interface to HERACLES [22]. The CDM approach is simulated using tuned parameters according to [23]. The LEPTO program allows the simulation of soft colour interactions (SCI) [24], through which the production of diffraction-like configurations is enhanced via non-perturbative colour rearrangements between the outgoing partons. The DJANGO MC simulations are calculated using the H1PDF 2009 parameterisation [25] of the parton distribution in the proton. In the following, the predictions based on LEPTO and ARIADNE are denoted LEPTO and CDM, respectively.

The contribution from proton dissociation, where the forward particles originate from the decay of a higher mass state, is estimated using an implementation in the RAPGAP [26] program of the dissociation model originally developed for the DIFFVM [27] MC generator. It amounts to about 30% at low x_L values decreasing to 10% at high x_L . This contribution is comparable to the contribution of SCI in LEPTO.

An additional weight as function of x_L is applied to the generated distributions, so that the relevant reconstructed kinematic distributions are well described throughout the phase space of the measurement.

The measured distributions may contain background arising from several sources. The background from photoproduction processes, where the positron is scattered into the backward beam-pipe and a particle from the hadronic final state fakes the positron signature in the SpaCal, is estimated using the PHOJET MC generator [28] and found to be negligible. The selected sample may contain background from neutrons, which at low energies can be reconstructed as electromagnetic clusters. This background is also found to be negligible according

to the MC simulation. Background also arises from the random coincidence of DIS events, which cause activity in the central detector, with a signal in the FNC which originates from the interactions of other beam protons with positrons or with residual gas in the beampipe. This contribution is estimated by combining DIS events with forward particles originating from the interactions in the bunch-crossings adjacent to the bunch-crossing of the DIS event. It is found to be smaller than 1%. The estimated background contributions are not subtracted from the measurements.

Correction factors are determined from the MC simulations as the ratio of the cross section obtained at hadron level to the cross section calculated using reconstructed particles and including the effects of QED radiation from the positron. For cross section calculations, the MC correction factors are applied to the measured data distributions bin-by-bin. The size of the correction factors varies between 3.5 to 2 for x_L^{lead} , between 3 to 4 for x_L^{sum} and between 3 to 10 for p_T^{lead} . The correction factors take into account the non-uniform azimuthal acceptance of the FNC, which is about 30% on average. The bin purities, defined as the fraction of events reconstructed in a particular bin that originate from that bin on hadron level, are between 75% and 95%. The bin stabilities, defined as the fraction of events originated from a particular bin on hadron level that are reconstructed in that bin, are typically higher than 60%, except at the highest x_L and p_T values, where they drop to 40%. This is due to the limited geometrical acceptance of the FNC.

3.4 Systematic uncertainties on the measured cross sections

Several sources of experimental uncertainties and their effect on the measured cross sections have been considered and quantified. The systematic uncertainties on the cross section measurements are determined using MC simulations, by propagating the corresponding estimated measurement uncertainty through the full analysis chain.

As the cross sections are presented normalised to the inclusive DIS cross sections measured in this analysis, some important systematic uncertainties related to the reconstruction of the scattered positron and the hadronic final state, the trigger efficiency and luminosity are largely reduced or cancel. The dominant uncertainties are from the electromagnetic energy scale of the FNC, the uncertainty of the impact position of the photon on the FNC and the model dependence of corrections. These effects are strongly correlated between measurement intervals and mainly contribute to the overall normalisation uncertainty.

The systematic errors shown in the figures are calculated as the quadratic sum of all contributions, which may vary from point to point.

4 Results

The measured DIS cross sections for very forward photon production, normalised to the total inclusive DIS cross sections, in the kinematic range $6 < Q^2 < 100 \text{ GeV}^2$ and $0.05 < y < 0.6$ are presented in Figs. 2-4.

The measured differential cross sections are presented in Figs. 2 and 3 as a function of the longitudinal momentum fraction x_L^{lead} and the transverse momentum p_T^{lead} of the most energetic photon with $0.1 < x_L < 0.7$ in the pseudorapidity range $\eta > 7.9$. The pseudorapidity of the photon is calculated in the H1 laboratory frame.

The MC simulations indicate that at low energies the clusters reconstructed in the FNC mainly originate from single photons. The contribution from two or more photons increases to 10% at about 450 GeV and to 80% at 900 GeV. Therefore, at relatively low energies, the measurement may be interpreted as a measurement of a leading photon in the angular range defined by the geometrical acceptance of the detector, while at higher energies the measurement represents total forward photon production. The cross section is also presented as a function of the sum of longitudinal momentum fractions x_L^{sum} of all photons with $\eta > 7.9$ in Fig. 4.

The data are compared with the predictions of models for inclusive DIS (LEPTO and CDM), and with the predictions of hadronic interaction models (EPOS, SIBYLL and QGSJET). The ratios of MC model predictions to the measurement are shown separately. In all these models, the main source of forward photons is the decay of π^0 -mesons produced from the hadronisation of the proton remnant. Forward photons can also be produced from different processes, e.g. they may be radiated from the beam proton or quarks. These processes are not included in the MC simulations, but the contribution from these process is expected to be small in the measured x_L range.

All models used in this paper overestimate the total rate of forward photons. The LEPTO and CDM models predict about 70% more photons than measured, while EPOS, SIBYLL and QGSJET overestimate the rate of photons by about 50%.

The shapes of all measured distributions are very well described by LEPTO, while the CDM description is very poor and degrades rapidly with increasing x_L or p_T .

The EPOS and SIBYLL models give fairly similar predictions to one another, as do the QGSJET predictions. The QGSJET models describe the x_L dependence of the data except at the lowest x_L , while the EPOS and SIBYLL models fail. The p_T dependence of the data lies between the four model predictions, except at the lowest p_T where all models overestimate the cross section.

5 Summary

The production of highly energetic forward photons has been studied in deep-inelastic positron-proton scattering in the kinematic region $6 < Q^2 < 100 \text{ GeV}^2$, $0.05 < y < 0.6$. The normalised DIS cross sections of production of the most energetic photon $1/\sigma_{DIS} d\sigma/dx_L^{lead}$, $1/\sigma_{DIS} d\sigma/dp_T^{lead}$ with $0.1 < x_L < 0.6$ and the pseudorapidity range $\eta > 7.9$ and the sum of photons $1/\sigma_{DIS} d\sigma/dx_L^{sum}$ in the range $\eta > 7.9$ are presented. Predictions of Monte Carlo models overestimate the rate of photons. The shapes of measured cross sections are well described by the LEPTO MC simulation, while the CDM model fails especially at high x_L or p_T . The QGSJET models provide reasonable descriptions of the x_L dependence of the data while the EPOS and SIBYLL models provide a similar level of description of the p_T dependence.

References

- [1] C. Adloff *et al.* [H1 Collaboration], Eur. Phys. J. **C6**, 587 (1999), [hep-ex/9811013].
- [2] S. Chekanov *et al.* [ZEUS Collaboration], Nucl. Phys. **B637**, 3 (2002), [hep-ex/0205076].
- [3] J. Breitweg *et al.* [ZEUS Collaboration], Nucl. Phys. **B596**, 3 (2001), [hep-ex/0010019].
- [4] S. Chekanov *et al.* [ZEUS Collaboration], Phys. Lett. **B610**, 199 (2005), [hep-ex/0404002].
- [5] A. Aktas *et al.* [H1 Collaboration], Eur. Phys. J. **C41**, 273 (2005), [hep-ex/0501074].
- [6] S. Chekanov *et al.* [ZEUS Collaboration], Phys. Lett. **B590**, 143 (2004), [hep-ex/0401017].
- [7] S. Chekanov *et al.* [ZEUS Collaboration], Nucl. Phys. **B776**, 1 (2007), [hep-ex/0702028].
- [8] S. Chekanov *et al.* [ZEUS Collaboration], JHEP **06**, 074 (2009), [0812.2416].
- [9] F. D. Aaron *et al.* [H1 Collaboration], Eur. Phys. J. **C68**, 381 (2010), [arXiv:1001.0532].
- [10] K. Charchula, G. A. Schuler and H. Spiesberger, Comput. Phys. Commun. **81**, 381 (1994), DJANGO 1.4.
- [11] K. Werner, F.-M. Liu and T. Pierog, Phys. Rev. **C74**, 044902 (2006), [hep-ph/0506232].
- [12] N. N. Kalmykov and S. S. Ostapchenko, Phys. Atom. Nucl. **56**, 346 (1993).
- [13] N. N. Kalmykov, S. S. Ostapchenko and A. I. Pavlov, Nucl. Phys. Proc. Suppl. **52B**, 17 (1997).
- [14] S. Ostapchenko, Phys. Rev. **D74**, 014026 (2006), [hep-ph/0505259].
- [15] S. Ostapchenko, AIP Conf. Proc. **928**, 118 (2007), [arXiv:0706.3784].
- [16] J. Engel, T. K. Gaisser, T. Stanev and P. Lipari, Phys. Rev. **D46**, 5013 (1992).
- [17] E.-J. Ahn *et al.*, Phys. Rev. **D80**, 094003 (2009), [arXiv:0906.4113].
- [18] R. Brun *et al.*, *GEANT: simulation program for particle physics experiment. User guide and reference manual*, CERN-DD-78-2-REV.
- [19] G. Ingelman, A. Edin and J. Rathsman, Comput. Phys. Commun. **101**, 108 (1997), [hep-ph/9605286], LEPTO 6.5.
- [20] L. Lönnblad, Comput. Phys. Commun. **71**, 15 (1992), ARIADNE 4.10.
- [21] B. Andersson *et al.*, Phys. Rept. **97**, 31 (1983).
- [22] A. Kwiatkowski, H. Spiesberger and H. J. Möhring, Comp. Phys. Commun. **69**, 155 (1992).

- [23] A. Aktas *et al.* [H1 Collaboration], Eur. Phys. J. **C46**, 27 (2006), [hep-ex/0508055].
- [24] A. Edin, G. Ingelman and J. Rathsman, Phys. Lett. **B366**, 371 (1996), [hep-ph/9508386].
- [25] F. D. Aaron *et al.* [H1 Collaboration], Eur. Phys. J. **C64**, 561 (2009), [arXiv:0904.3513].
- [26] H. Jung, Comp. Phys. Commun. **86**, 147 (1995), RAPGAP 3.1.
- [27] B. List and A. Mastroberardino, *DIFFVM: A Monte Carlo generator for diffractive processes in ep scattering*, in: A.T. Doyle *et al.* ed., "Monte Carlo generators for HERA physics, proceedings of the workshop 1998-1999," Hamburg (DESY) DESY-PROC-1999-02, p. 396-404.
- [28] R. Engel and J. Ranft, Phys. Rev. **D54**, 4244 (1996), [hep-ph/9509373].

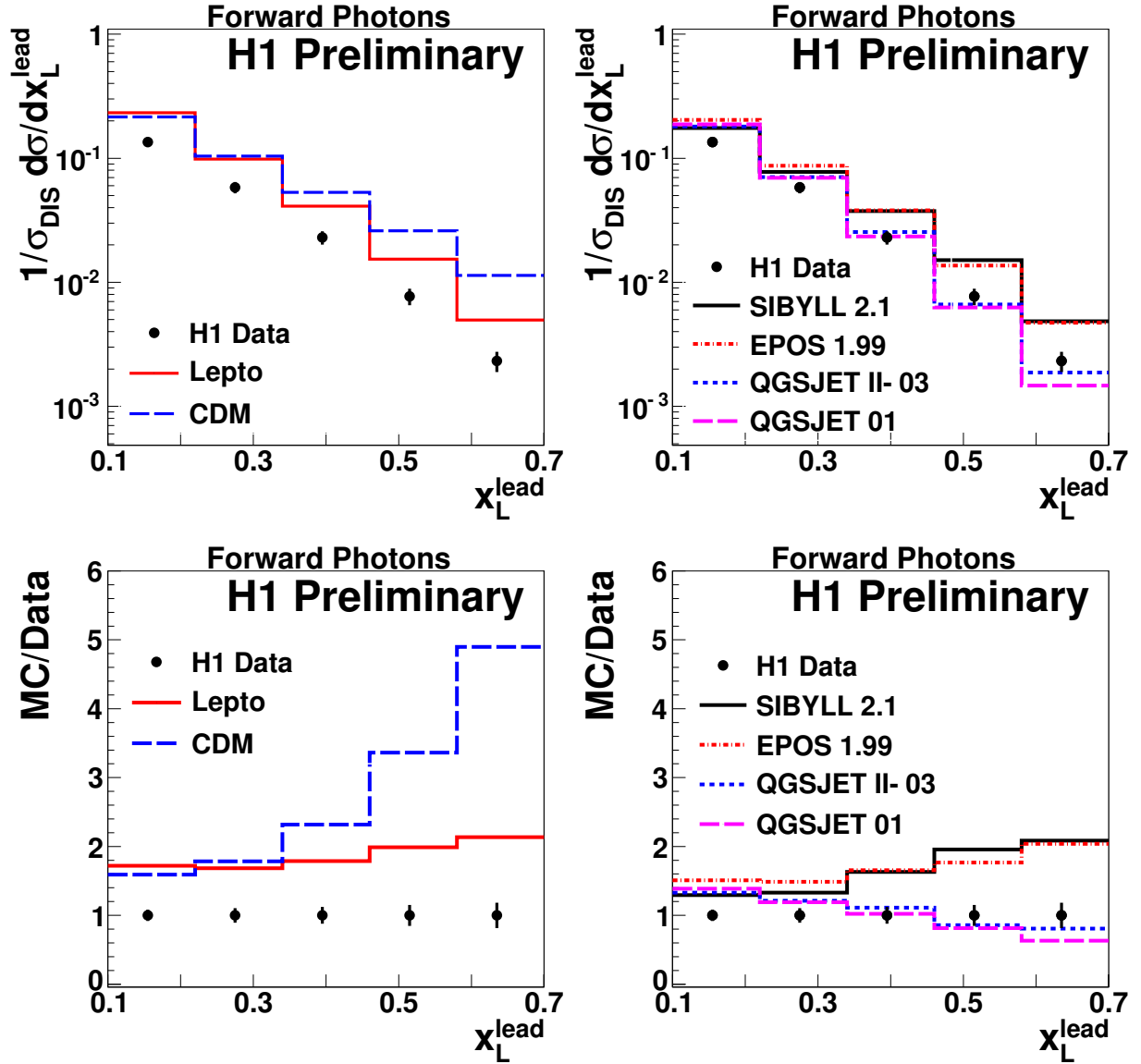


Figure 2: The normalised cross sections of forward photon production in deep-inelastic scattering in the kinematic range $6 < Q^2 < 100 \text{ GeV}^2$ and $0.05 < y < 0.6$ as a function of the fractional energy x_L^{lead} of the leading photon in the energy range $0.1 < x_L < 0.7$ and the pseudorapidity range $\eta > 7.9$. The data are compared to the predictions of the DJANGO Monte Carlo simulations, using LEPTO and CDM for higher order simulation, and the hadronic interaction models QGSJET, EPOS and SIBYLL. The lower plots show the ratios of the Monte Carlo predictions to the data. The inner error bars show the statistical uncertainties and the outer error bars show the quadratic sum of the statistical and systematic uncertainties.

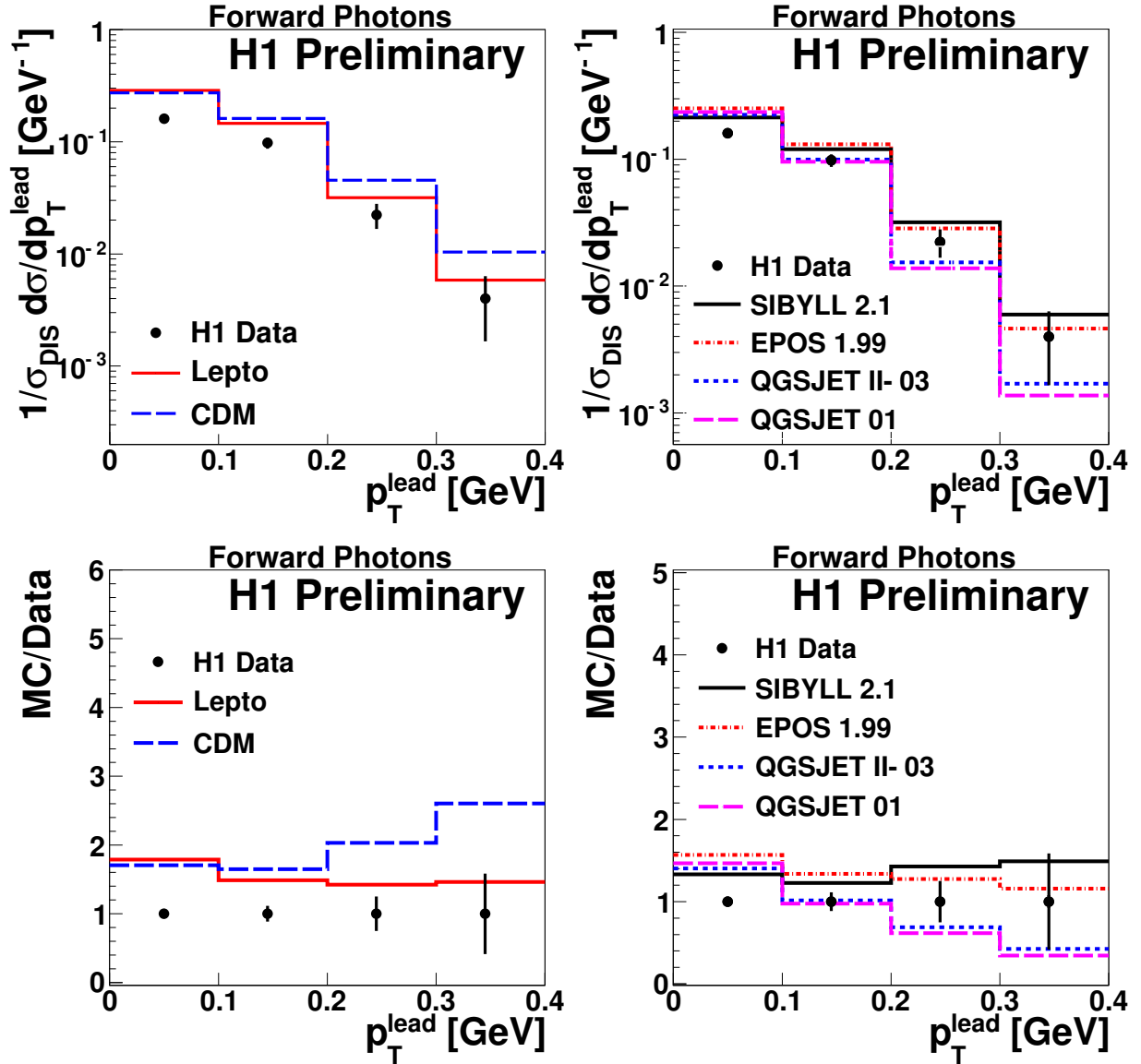


Figure 3: The normalised cross sections of forward photon production in deep-inelastic scattering in the kinematic range $6 < Q^2 < 100 \text{ GeV}^2$ and $0.05 < y < 0.6$ as a function of the transverse momentum p_T^{lead} of the leading photon in the energy range $0.1 < x_L < 0.7$ and the pseudorapidity range $\eta > 7.9$. The data are compared to the predictions of the DJANGO Monte Carlo simulations, using LEPTO and CDM for higher order simulation, and the hadronic interaction models QGSJET, EPOS and SIBYLL. The lower plots show the ratios of the Monte Carlo predictions to the data. The inner error bars show the statistical uncertainties and the outer error bars show the quadratic sum of the statistical and systematic uncertainties.

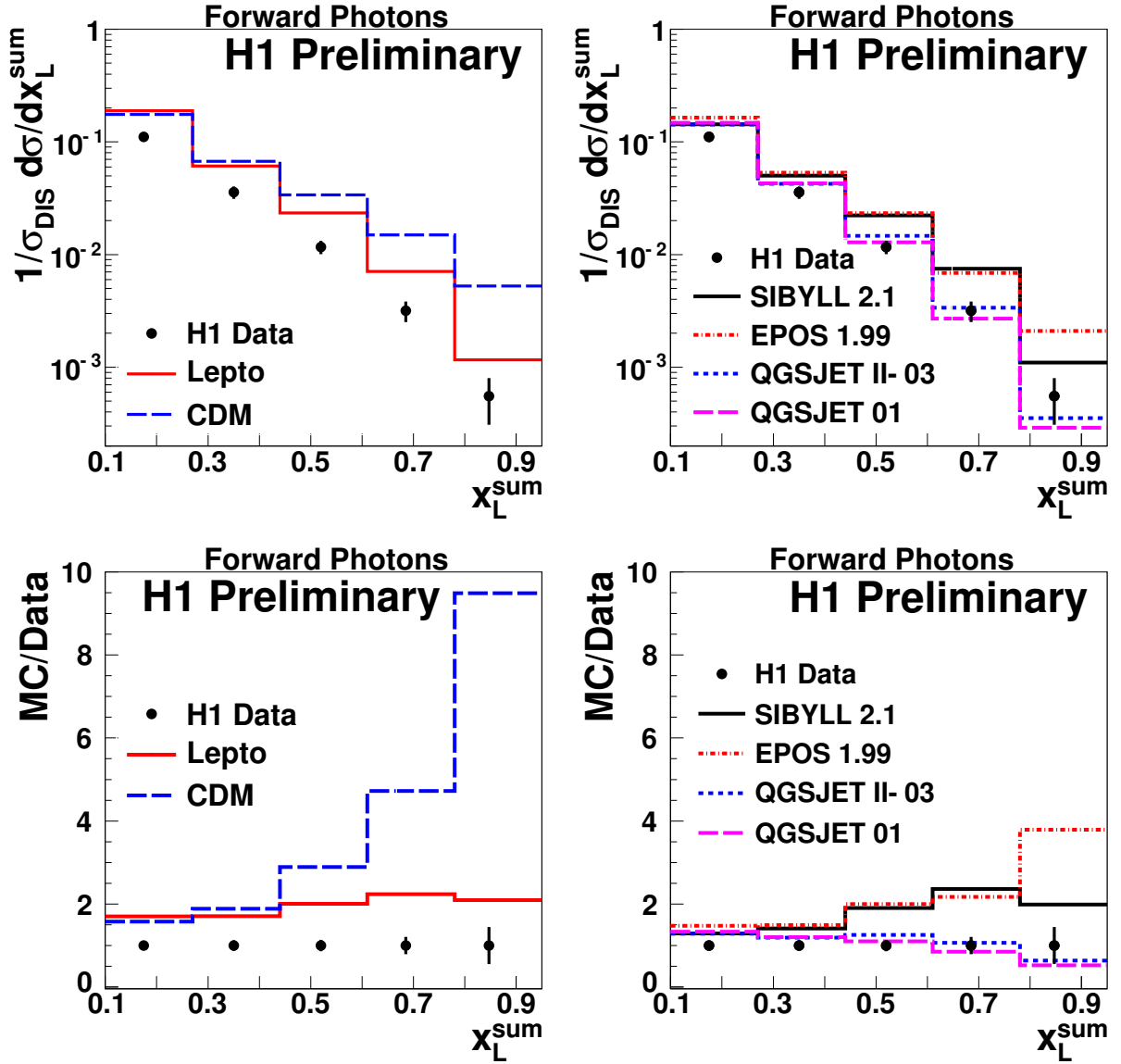


Figure 4: The normalised cross sections of forward photon production in deep-inelastic scattering in the kinematic range $6 < Q^2 < 100 \text{ GeV}^2$ and $0.05 < y < 0.6$ as a function of the sum of the fractional energies of photons x_L^{sum} in the pseudorapidity range $\eta > 7.9$. The data are compared to the predictions of the DJANGO Monte Carlo simulations, using LEPTO and CDM for higher order simulation, and the hadronic interaction models QGSJET, EPOS and SIBYLL. The lower plots show the ratios of the Monte Carlo predictions to the data. The inner error bars show the statistical uncertainties and the outer error bars show the quadratic sum of the statistical and systematic uncertainties.